This article appeared as:
K. Makino and S. Biwa, Influence of axle–wheel interface on ultrasonic testing of fatigue cracks in wheelset, Ultrasonics, Vol. 53 (2013), pp. 239–248.

Influence of Axle–Wheel Interface on Ultrasonic Testing of Fatigue Cracks in Wheelset

Kazunari Makino [a] and Shiro Biwa [b]

a: *Vehicle Structure Technology Division, Railway Technical Research Institute, 2-8-38, Hikari-cho, Kokubunji-shi, Tokyo 185-8540, Japan*

b: *Department of Aeronautics and Astronautics, Graduate School of Engineering, Kyoto University, Katsura, Nishikyo-ku, Kyoto 615-8540, Japan*

Corresponding author: Kazunari Makino (makino.kazunari.34@rtri.or.jp)

Abstract

For the ultrasonic testing at the wheel seat of railway axles, quantitative investigation of the reflection and transmission phenomena at the axle–wheel interface is important. This paper describes the influence of the axle–wheel interface on the ultrasonic testing of a fatigue crack in a wheelset by applying the spring interface model. The normal and tangential stiffnesses were identified experimentally for an as-manufactured wheelset at the normal incidence, and the reflection coefficient for the shear-wave oblique incidence was calculated. A parametric study was performed to clarify the influence of these interfacial stiffnesses on the incident-angle dependence of the reflection coefficient. The calculated reflection coefficient at the incident angle of 45 degrees qualitatively explained the relative echo-height decrease due to the presence of a wheel observed experimentally for a wheelset in fatigue loading by rotating bending. The quantitative difference between the experimental and calculated results was considered to be due to the reduction of the effective interference of shrink fit by the wear at the axle–wheel interface during the fatigue loading as well as by the applied bending moment. For the estimated relative echo-height decrease to agree with the experimental results, the interfacial stiffnesses were found to be smaller than the values identified for the as-manufactured wheelset by a factor of 0.5 to 0.7.

Keywords: Railway wheelset; Axle–wheel interface; Spring interface model; Interfacial stiffness; Reflection coefficient; Shear-wave oblique incidence

1. Introduction

Railway axles are inspected periodically by a certain time interval or a certain running distance by means of the ultrasonic testing and/or the magnetic particle testing [1, 2]. When the ultrasonic testing of a railway axle is performed, attentions are to be paid to the respective positions where the components such as a wheel, a gear, a bearing and a brake disk are fitted [3, 4]. Among them, the position where a wheel is fitted, i.e. the wheel seat on the axle, is a potential site for the development of a fatigue crack initiated by the effect of fretting [5, 6], which motivates the careful inspection at the wheel seat.

In the ultrasonic testing at the wheel seat, it is expected that a flaw echo might be affected by the contact between the axle and the wheel [7, 8], since the axle–wheel contact interface transmits some portion of the ultrasound which reached the vicinity of a crack into the wheel. The behavior of the ultrasound in the testing with the shear-wave angle beam, whose incident angle is around 37 to 55 degrees in most cases, is schematically shown in Fig. 1. It involves the reflection and transmission phenomena at the axle–wheel interface as well as at the faces of a possibly closed fatigue crack. Quantitative investigation of these phenomena is currently not sufficient, in spite of importance to understand the effect of a fitted wheel on the inspection accuracy.

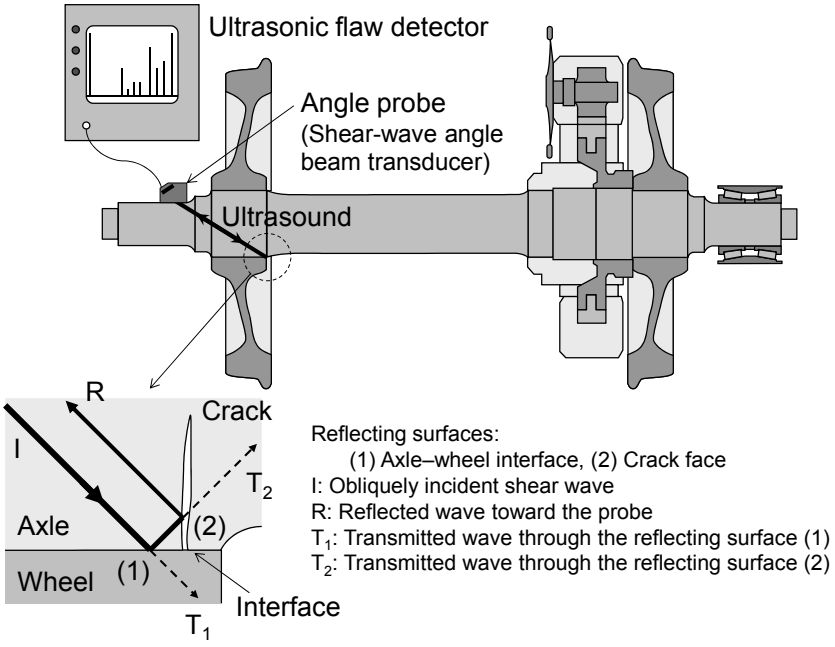

Fig. 1. Schematic view of the ultrasonic testing with shear-wave angle probes.

In the previous report [9], it was clarified that the echo height of a fatigue crack at the wheel seat in the ultrasonic experiment was significantly reduced by the presence of a wheel. Therefore, in this paper, we discuss the influence of the axle–wheel interface on the ultrasonic testing of a fatigue crack in a wheelset in a more quantitative manner, by applying the spring interface model [10–12]. For this purpose, the normal and tangential stiffnesses of the axle–wheel interface are identified experimentally from the measurement of the reflection coefficient of longitudinal and shear waves for the normal incidence, by using a miniature wheelset having the dimensions similar to the one used for the ultrasonic experiment of the fatigue crack.

With the identified interfacial stiffnesses, the reflection coefficient at the axle–wheel interface for the shear-wave oblique incidence is calculated theoretically as a function of the incident angle. A parametric study is performed to clarify the influence of the interfacial stiffnesses on the incident-angle dependence of the reflection coefficient. Based on the results of these theoretical calculations, we attempt to explain the relative decrease of the echo height of a fatigue crack by the presence of a wheel.

2. Ultrasonic test results for fatigue crack

First, we explain an overview of the ultrasonic testing of a fatigue crack in a miniature wheelset test piece as reported in Ref. [9]. Although the experimental study described in this reference involved two types of ultrasound incidence (angled shear wave and grazing shear-horizontal wave) and two fatigue cracks with different depths, only the results pertinent to the present discussion are outlined here. A schematic view of the test piece and the test setup is shown in Fig. 2(a). Both of the axle and the wheel were manufactured from carbon steel. The diameter of the wheel seat (fitting part) of the axle was 57 mm, and the wheel with the outer diameter of 87 mm was shrink fitted on the wheel seat. An interference set between the axle and the wheel generated the contact pressure of approximately 85 MPa, which was similar to that for full-sized wheelsets. According to the measurement of the surface roughness profile, the maximum height of profile at the surface of the axle was approximately 3 μm and that at the inner bore of the wheel was approximately 10 μm.

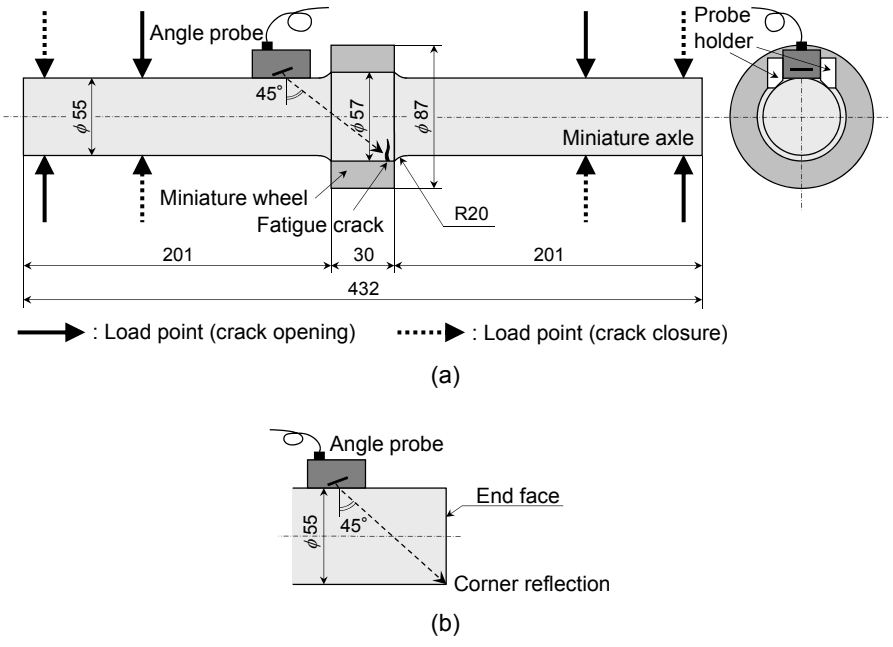

Fig. 2. Schematic view of (a) the test setup for a miniature wheelset and (b) the measurement of the corner reflection for the normalization of the echo height.

A fatigue crack was developed on the surface of the wheel seat by using a four-point rotating bending fatigue test machine. This fatigue crack was initiated by the effect of fretting at the axle–wheel interface and developed from the surface of the wheel seat as an ordinary fatigue crack under bending. A destructive measurement was performed after all the ultrasonic test menus mentioned below were completed. It was found that the fatigue crack had an actual depth of 3.5 mm and the distance of the crack from the edge of the wheel seat was around 0.7 mm.

A load cycle was applied to vary the nominal stress σ_n at the surface of the wheel seat in the order of 0, +165, 0, –165 and 0 MPa, where σ_n was calculated by the bending moment M and the diameter of the wheel seat d as $\sigma_n = M / (\pi d^3 / 32)$. The ultrasonic testing was performed to measure the flaw echo height in each state of the crack opening and closure. Two ultrasonic angle probes (shear-wave angle beam transducers) with the refraction angle of 45 degrees were used, each of which had the nominal frequency of 2 or 5 MHz. Next, we removed the wheel by cutting it, and performed the same menus of ultrasonic testing for the axle without a wheel. The echo heights were normalized by the reflection at the corner of axle end face as shown in Fig. 2(b).

The normalized echo heights of the fatigue crack are plotted in Fig. 3 against the nominal stress at the wheel seat in the process of increasing and decreasing σ_n. For each nominal frequency, the echo heights were compared between two cases, namely, the case 1 where the axle was fitted with a wheel and the case 2 where the wheel was cut off from the axle. The echo height saturated when the tensile stress was higher than approximately 50 MPa, since the state of the fatigue crack approached that of an open flaw. We calculated the relative decrease of the echo height from the case 2 (without a wheel) to the case 1 (with a wheel), in the state where the nominal tensile stress of +165 MPa was applied at the wheel seat to open the crack faces. As shown in Fig. 3, the relative decrease was 13.1 dB at 2 MHz and 9.2 dB at 5 MHz. This echo-height reduction was considered to be due to the contact between the axle and the wheel. Therefore, it is the aim of the present paper to examine it in a quantitative manner by applying a theoretical model to the axle–wheel interface.

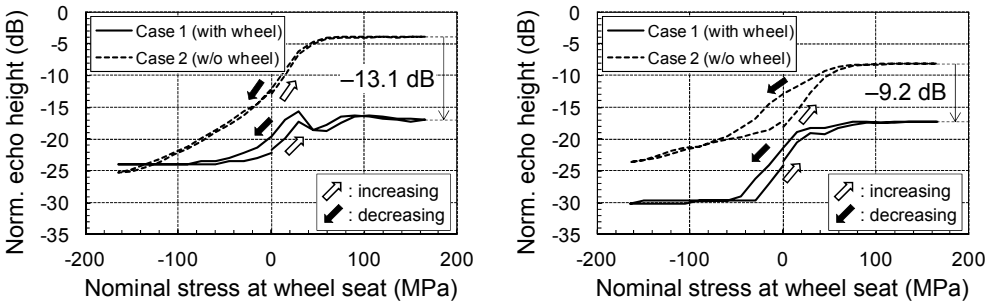

Fig. 3. The echo-height variation of the fatigue crack with the nominal stress at the wheel seat for increasing (–165 → 0 → +165 MPa) and decreasing (+165 → 0 → –165 MPa) nominal stress, for (a) 2 MHz and (b) 5 MHz.

3. Identification of interfacial stiffnesses by normal incident wave

3.1. Theoretical background

In this paper, we attempt to discuss the results of the echo-height measurement mentioned above by modeling the axle–wheel interface theoretically as a combination of normal and tangential springs [13]. The schematic view of the spring interface model is shown in Fig. 4. The normal and tangential stiffnesses, K_N and K_T respectively, are introduced to express the behavior of the ultrasound propagation under the contact pressure, which is generated by the interference between the wheel bore and the wheel seat of the axle. These stiffnesses correspond to the increment of the normal or shear stress generated when the relative distance between two media, i.e. the axle and the wheel, varied by a unit length in each direction.

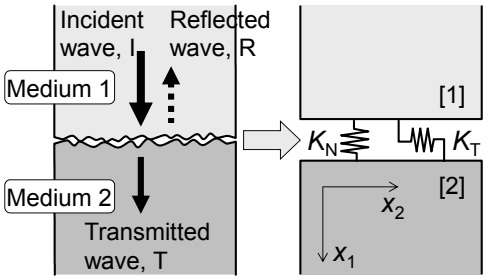

Fig. 4. A schematic view of the spring interface model.

When the longitudinal wave with the angular frequency ω is incident to the interface from medium 1 to medium 2 in the normal direction taken in the x_1 axis, the reflection coefficient R_L of the longitudinal wave is defined as the ratio of the displacement amplitude of the reflected wave to that of the incident wave, and given by [14, 15]

$$R_L = \left| \frac{W_{L1} - W_{L2} - \dfrac{i\omega W_{L1} W_{L2}}{K_N}}{W_{L1} + W_{L2} - \dfrac{i\omega W_{L1} W_{L2}}{K_N}} \right|, \tag{1}$$

where W_{Li} is the longitudinal acoustic impedance in each medium (i = 1, 2).

In the special case where the two media consist of the same material, i.e. $W_{L1} = W_{L2} \equiv W_L$, we obtain the following expression to acquire the normal stiffness K_N from the reflection coefficient R_L,

$$K_N = \frac{\omega W_L}{2} \sqrt{\frac{1}{R_L^{\,2}} - 1}\,, \quad W_L = \rho c_L \tag{2}$$

where ρ and c_L are the density and the longitudinal wave velocity, respectively, of the two media.

Likewise, for the normal incidence of the shear wave, we obtain the following expression to acquire the tangential stiffness K_T from the reflection coefficient R_T,

$$K_T = \frac{\omega W_T}{2} \sqrt{\frac{1}{R_T^{\,2}} - 1}\,, \quad W_T = \rho c_T \tag{3}$$

where W_T and c_T are the shear wave acoustic impedance and the corresponding wave velocity.

3.2 Experimental procedure

In order to identify the normal and tangential stiffnesses of the axle–wheel interface, K_N and K_T respectively, we performed the measurements of the reflection coefficients [16] by using a miniature wheelset test piece as shown in Fig. 5. This test piece has similar dimensions including the interference between the wheel bore and the wheel seat, and consequently comparable conditions of the axle–wheel interface, with the wheelset having fatigue cracks inspected by obliquely incident shear wave as described in Section 2.

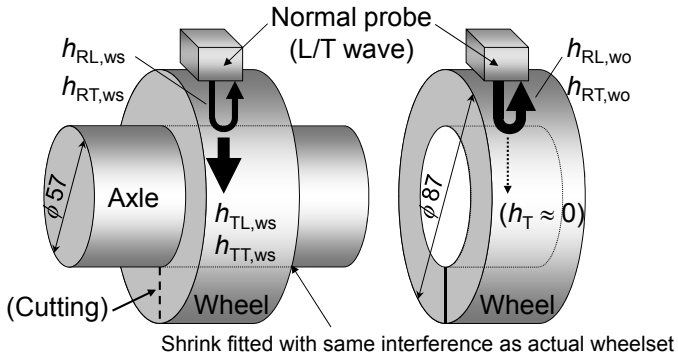

Fig. 5. Measurement of reflected echo heights at the axle–wheel interface by using miniature wheelset.

At first, a longitudinal-wave normal probe was placed on the outer surface of the wheel as shown on the left side of Fig. 5, and the reflected wave at the axle–wheel interface was recorded and converted into the frequency domain by the fast Fourier transformation. Consequently, the amplitude spectrum of the reflected wave for a wheel fitted on the axle, $h_{RL,ws}(f)$ (ws: wheelset), was obtained as a function of the frequency f. Next, the wheel was cut at a position opposite to the probed area and the axle was removed from the wheel, and as shown on the right side of Fig. 5, the amplitude spectrum of the reflected wave at the free surface of the bore of the wheel, $h_{RL,wo}(f)$ (wo: wheel only), was obtained as a function of the frequency f. The second measurement was performed by placing the probe at the same place on the outer surface of the wheel as that of the first measurement.

The reflection coefficient of the longitudinal wave R_L, which is defined in Eq. (1), is obtained at each frequency as the ratio of the two echo-height spectra:

$$R_L(f) = \frac{h_{RL,ws}(f)}{h_{RL,wo}(f)}. \tag{4}$$

It is noted here that both $h_{RL,ws}(f)$ and $h_{RL,wo}(f)$ contain the effect of the wheel curvatures. When defined in the above manner, however, the curvature effect on the obtained reflection coefficient can be cancelled out and kept minimal.

In the same way, we can acquire the reflection coefficient of the shear wave R_T by using a shear-wave normal probe. Here, the probe was placed at the outer surface of the wheel to adjust the vibration direction of the transducer to the axial direction of the test piece. R_T is calculated as a function of the frequency from the two echo-height spectra of $h_{RT,ws}(f)$ and $h_{RT,wo}(f)$ by

$$R_T(f) = \frac{h_{RT,ws}(f)}{h_{RT,wo}(f)}. \quad (5)$$

By substituting the values of R_L and R_T into Eqs. (2) and (3), the normal and tangential stiffnesses can be identified for the axle–wheel interface with a specific interference as a function of the frequency.

An ultrasonic flaw detector USN 60 (GE Sensing & Inspection Technologies) was used for the measurement: the frequency range was 0.25–25 MHz, the maximum amplifier gain was 110 dB, and the pulser was the spike pulse with the damping resistor of 50 Ω.

To obtain the reflection coefficients R_L and R_T in a wide frequency range, we used two normal probes, with the nominal frequency of 2 and 5 MHz, for both of the longitudinal and shear wave reflection measurements. Detailed specifications of the probes are shown in Table 1. A special couplant for the shear wave SONICOAT SHN-B25 (Saan-Tech Corporation) with the viscosity of 115 Pa·s at 20 °C was used for both of the longitudinal and shear wave reflection measurements to acquire stable data under the contact between the probe and the curved surface of the wheel [17]. We measured the echo heights at three positions on the wheel surface with each probe and the averaged reflection coefficients were used to calculate the interfacial stiffnesses in the frequency domain.

Table 1. Probes used for the measurement of reflection coefficients.

No.	Wave mode	Nominal frequency (MHz)	Band width	Transducer diameter (mm)	Product name
1	Longitudinal	2	Broad	20	Japan Probe, B2C20N
2	Longitudinal	5	Broad	10	Japan Probe, B5C10N
3	Shear	2	Narrow	10	KGK, 2C10SN
4	Shear	5	Narrow	10	KGK, 5C10SN

3.3 Identified values of interfacial stiffnesses

Figures 6(a) and (b) show typical examples of the amplitude spectra of the reflected longitudinal waves, $h_{RL,ws}(f)$ and $h_{RL,wo}(f)$, around the nominal frequency of the 2 and 5 MHz probes. The reflection coefficient of the longitudinal wave in the frequency domain $R_L(f)$, calculated by Eq. (4), is shown in Fig. 6(c). Figure 6(d) shows the interfacial normal stiffness K_N calculated by Eq. (2). From Figs. 6(c) and (d), the value of R_L at 2 MHz is approximately 0.159 and $K_N = 1.82 \times 10^{15}$ N/m^3. In the same way, the values of $R_L = 0.328$ and $K_N = 2.11 \times 10^{15}$ N/m^3 are obtained at 5 MHz. Figure 7 shows the experimental results acquired by the shear-wave probes. By referring to the Figs. 7(c) and (d), $R_T = 0.459$ and $K_T = 3.24 \times 10^{14}$ N/m^3 are obtained at 2 MHz, and $R_T = 0.575$ and $K_T = 5.70 \times 10^{14}$ N/m^3 are obtained at 5 MHz.

Marshall et al. [8] presented the relation between the contact pressure p (MPa) and the solid interfacial stiffness K (GPa/μm) as $p = 51.72\,K$ for the press-fitted axle–wheel interface by using a normal probe with the frequency of 8.8 MHz. In applying this expression tentatively to our measurements, the value of the normal stiffness at 8.0 MHz by the 5 MHz probe, $K_N = 2.01 \times 10^{15}$ N/m^3 (2.01 GPa/μm), is substituted into this p–K equation, since the magnitude of the two amplitude spectra shown in Fig. 6(b) is not sufficient beyond 8 MHz. The resulting value of p is 104 MPa, which does not differ much from the actual contact

pressure of the miniature wheelset, i.e. approximately 85 MPa. This indicates that the K_N value obtained experimentally is reasonable. A better representation for our experiment is given by a formula $p = 46.7\ K_N$ at 2 MHz provided that the interfacial stiffness is proportional to the contact pressure.

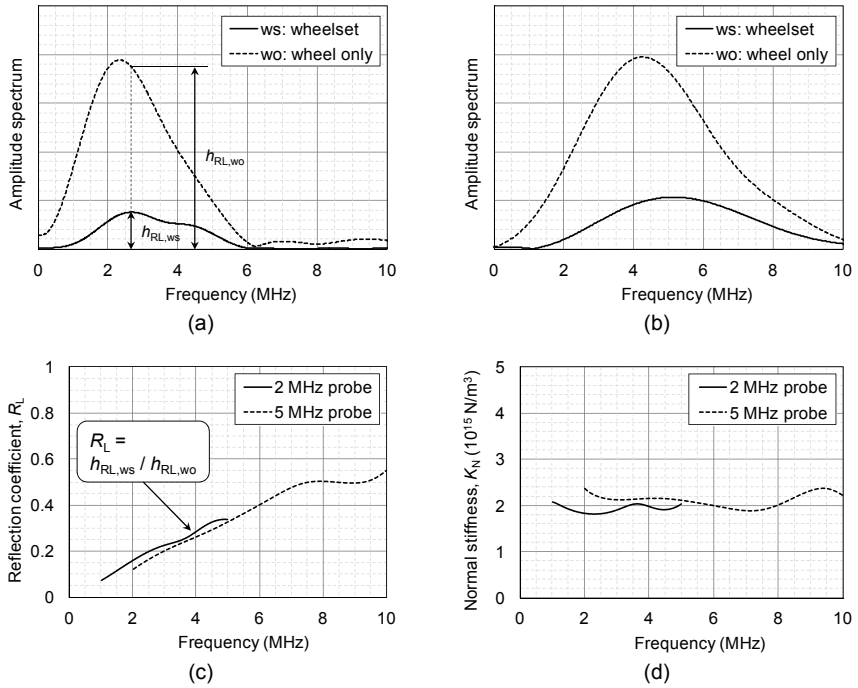

Fig. 6. Amplitude spectra of the reflected longitudinal waves with (a) 2 MHz probe and (b) 5 MHz probe, (c) reflection spectra of longitudinal normal wave, and (d) interfacial normal stiffness.

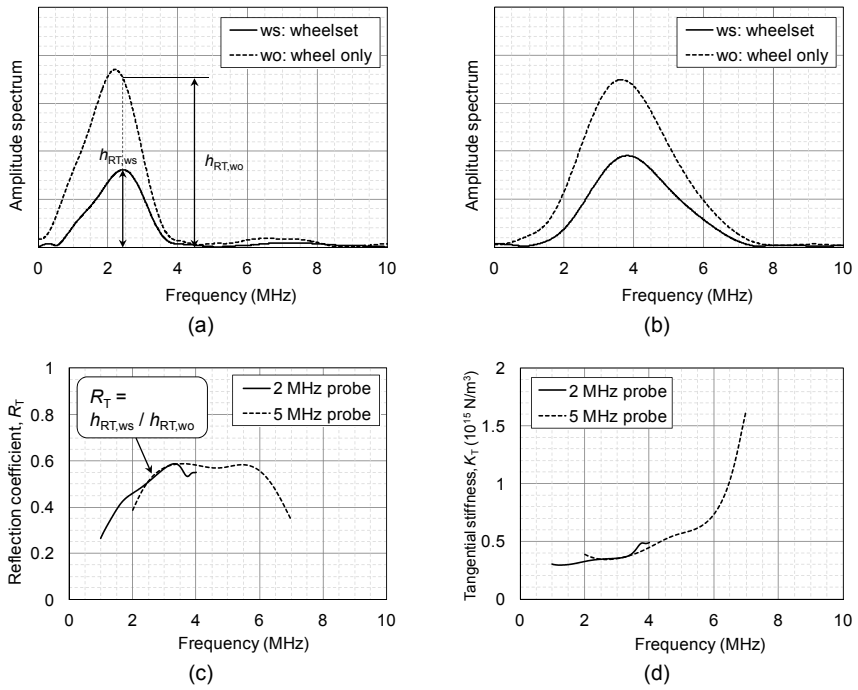

Fig. 7. Amplitude spectra of the reflected shear waves with (a) 2 MHz probe and (b) 5 MHz probe, (c) reflection spectra of shear normal wave, and (d) interfacial tangential stiffness.

It is noted that the peak frequency in the amplitude spectrum shown in Fig. 7(b) obtained by the 5 MHz shear-wave normal probe was around 3.7 MHz, which is substantially smaller than the nominal frequency of 5 MHz. This is considered to be due to the use of the special couplant mentioned above, which caused more significant attenuation of the higher frequency ultrasound. The values of R_T and K_T obtained by the spectra, however, are considered to be feasible up to 5 MHz or more as is shown in the continuity of the graphs in Figs. 7(c) and (d).

In the above identification, we used the measured sound velocities of the longitudinal and shear waves, c_L = 5,915 m/s and c_T = 3,235 m/s, respectively, and the typical value of the steel density ρ = 7,850 kg/m^3. The obtained values of K_N and K_T are summarized in Table 2. The ratio of the two stiffnesses, K_T / K_N, was 0.178 at 2 MHz and 0.270 at 5 MHz, respectively. These values are somewhat smaller than the values for the steel–steel interface reported in the foregoing studies [18, 19], which was around 0.30 in Ref. [18] for example.

Table 2. Identified values of interfacial stiffnesses.

Frequency, f (MHz)	Wave mode	Reflection coefficient, R_L, R_T	Interfacial stiffness, K_N, K_T (N/m^3)	K_T / K_N
2	Longitudinal	R_L = 0.159	K_N = 1.82 × 10^{15}	0.178
	Shear	R_T = 0.459	K_T = 3.24 × 10^{14}	
5	Longitudinal	R_L = 0.328	K_N = 2.11 × 10^{15}	0.270
	Shear	R_T = 0.575	K_T = 5.70 × 10^{14}	

4. Analysis of shear-wave reflection coefficient for oblique incidence to axle–wheel interface

4.1. Theoretical background

In this section, we consider the oblique incidence of the shear wave to the interface between two media (Lamé constants λ_i and μ_i, density ρ_i, and wave velocities c_{Li} and c_{Ti} with i = 1 and 2 for the medium 1 and 2, respectively), with interfacial stiffnesses K_N and K_T, as shown in Fig. 8. Since this problem has been analyzed by several authors [10–12], only the outline is described here. The displacement components of the incident shear wave (denoted by IT) with the amplitude $\bar{u}^{IT}$, the angular frequency ω, the wave number $k_{T1} = \omega/c_{T1}$ and the incident angle η_1 are expressed as

$$IT: \begin{pmatrix} u_1^{IT} \\ u_2^{IT} \end{pmatrix} = \bar{u}^{IT} \begin{pmatrix} -\ell_2 \\ \ell_1 \end{pmatrix} \exp\{i[k_{T1}(\ell_1 x_1 + \ell_2 x_2) - \omega t]\}, \tag{6}$$

where $\ell_1 = \cos\eta_1$ and $\ell_2 = \sin\eta_1$.

When η_1 is smaller than any critical angle(s), four kinds of waves are generated; the reflected longitudinal (RL) and the reflected shear (RT) waves with the reflection angles θ_1 and η_1 (same as the incident angle), and the transmitted longitudinal (TL) and the transmitted shear (TT) waves with the refraction angles θ_2 and η_2. The displacement components of these waves are expressed as

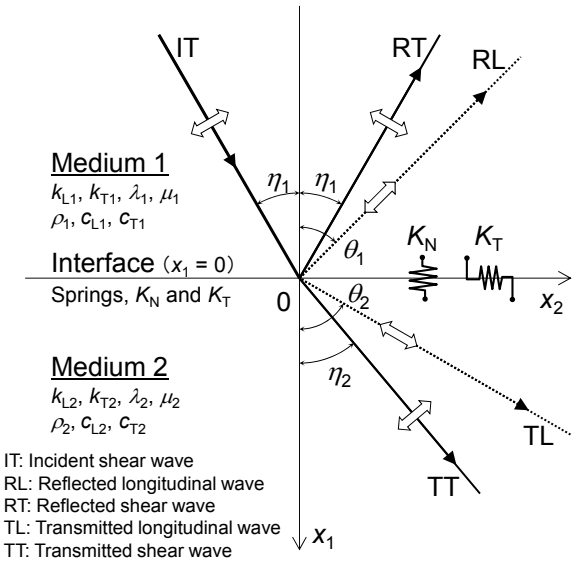

Fig. 8. Reflection and transmission of ultrasound at two-media interface.

$$RL: \quad \begin{pmatrix} u_1^{RL} \\ u_2^{RL} \end{pmatrix} = \bar{u}^{RL} \begin{pmatrix} -n_1 \\ n_2 \end{pmatrix} \exp\{i[k_{L1}(-n_1x_1 + n_2x_2) - \omega t]\}, \tag{7}$$

$$RT: \quad \begin{pmatrix} u_1^{RT} \\ u_2^{RT} \end{pmatrix} = \bar{u}^{RT} \begin{pmatrix} \ell_2 \\ \ell_1 \end{pmatrix} \exp\{i[k_{T1}(-\ell_1x_1 + \ell_2x_2) - \omega t]\}, \tag{8}$$

$$TL: \quad \begin{pmatrix} u_1^{TL} \\ u_2^{TL} \end{pmatrix} = \bar{u}^{TL} \begin{pmatrix} m_1 \\ m_2 \end{pmatrix} \exp\{i[k_{L2}(m_1x_1 + m_2x_2) - \omega t]\}, \tag{9}$$

$$TT: \quad \begin{pmatrix} u_1^{TT} \\ u_2^{TT} \end{pmatrix} = \bar{u}^{TT} \begin{pmatrix} -p_2 \\ p_1 \end{pmatrix} \exp\{i[k_{T2}(p_1x_1 + p_2x_2) - \omega t]\}, \tag{10}$$

where $k_{Li} = \omega/c_{Li}$, $k_{Ti} = \omega/c_{Ti}$ (i = 1, 2) and

$$\begin{aligned} &n_1 = \cos\theta_1, \;\; n_2 = \sin\theta_1, \\ &\ell_1 = \cos\eta_1, \;\; \ell_2 = \sin\eta_1, \\ &m_1 = \cos\theta_2, \;\; m_2 = \sin\theta_2, \\ &p_1 = \cos\eta_2, \;\; p_2 = \sin\eta_2. \end{aligned} \tag{11}$$

In the spring interface model, the boundary conditions are expressed by

$$\sigma_{11}^{[2]} = \sigma_{11}^{[1]} = K_N\left(u_1^{[2]} - u_1^{[1]}\right), \tag{12}$$

$$\sigma_{12}^{[2]} = \sigma_{12}^{[1]} = K_T\left(u_2^{[2]} - u_2^{[1]}\right), \tag{13}$$

at $x_1 = 0$, where σ_{11} and σ_{12} are the normal and shear stress components, and the superscript [1] or [2] indicates their values of medium 1 or 2. The total displacement components in each medium, $u_1^{[i]}$ and $u_2^{[i]}$ (i = 1, 2), are given by the sum of the above wave components, i.e. IT, RL and RT in medium 1 and TL and TT in medium 2. Enforcing these conditions first gives the following phase matching conditions,

$$k_{L1}n_2 = k_{T1}\ell_2 = k_{L2}m_2 = k_{T2}p_2. \tag{14}$$

Eqs. (12) and (13) are then reduced to the relations among the displacement amplitudes of IT, RL, RT, TL and TT, from which the amplitudes of the reflected and refracted waves can be obtained.

In the following discussion, we consider only the case where the medium 1 and 2 are identical, as this is reasonably valid in the present case where both of the axle and the wheel are manufactured from carbon

steel. Namely,

$$k_{L1} = k_{L2} \equiv k_L,\ k_{T1} = k_{T2} \equiv k_T,\ c_{L1} = c_{L2} \equiv c_L,\ c_{T1} = c_{T2} \equiv c_T,$$
$$\rho_1 = \rho_2 \equiv \rho,\ \lambda_1 = \lambda_2 \equiv \lambda,\ \mu_1 = \mu_2 \equiv \mu. \tag{15}$$

In this case, Eq. (14) leads to $m_2 = n_2$ and $p_2 = \ell_2$, and consequently, $\eta_2 = \eta_1$ and $\theta_2 = \theta_1$ from Eq. (11). Furthermore, there exists only one critical angle η_c, which is given by the following expression:

$$\eta_c = \sin^{-1}\frac{c_T}{c_L}. \tag{16}$$

When η_1 is beyond the critical angle η_c, approximately 33.2 degrees for steel, n_2 becomes greater than 1 from Eq. (14). In this case, there exists no real value of θ_1 which satisfies Eq. (11), and the value of n_1 is defined as an imaginary number by

$$n_1 \equiv in_1' = +i\sqrt{n_2^2 - 1}, \tag{17}$$

where n'_1 is a real number. Then, the longitudinal waves RL and TL become inhomogeneous waves which decay exponentially away from the interface.

When η_1 is below the critical angle η_c, Eqs. (12) and (13) yield

$$\begin{bmatrix} -k_L\left(\lambda+2\mu n_1^2\right) & 2k_T\mu\ell_1\ell_2 & k_L\left(\lambda+2\mu n_1^2\right) & -2k_T\mu\ell_1\ell_2 \\ 2k_L\mu n_1 n_2 & k_T\mu\left(\ell_1^2-\ell_2^2\right) & 2k_L\mu n_1 n_2 & k_T\mu\left(\ell_1^2-\ell_2^2\right) \\ K_N n_1 & -K_N\ell_2 & K_N n_1 - ik_L\left(\lambda+2\mu n_1^2\right) & -K_N\ell_2 + 2ik_T\mu\ell_1\ell_2 \\ -K_T n_2 & -K_T\ell_1 & K_T n_2 - 2ik_L\mu n_1 n_2 & K_T\ell_1 - ik_T\mu\left(\ell_1^2-\ell_2^2\right) \end{bmatrix} \begin{pmatrix} \bar{u}^{RL} \\ \bar{u}^{RT} \\ \bar{u}^{TL} \\ \bar{u}^{TT} \end{pmatrix} = \begin{pmatrix} -2k_T\mu\ell_1\ell_2 \\ k_T\mu\left(\ell_1^2-\ell_2^2\right) \\ -K_N\ell_2 \\ K_T\ell_1 \end{pmatrix} \bar{u}^{IT}. \tag{18}$$

This set of equations can be solved by numerical means to obtain $\bar{u}^{RL}$, $\bar{u}^{RT}$, $\bar{u}^{TL}$ and $\bar{u}^{TT}$ for a given $\bar{u}^{IT}$. When η_1 is beyond the critical angle η_c, n_1 is replaced by in'_1 in the above set of equations. Then, the reflection coefficient of the shear wave R_T can be calculated as the absolute value of $\bar{u}^{RT}/\bar{u}^{IT}$ as a function of the incident angle η_1.

4.2 Calculated results of reflection coefficient

Table 3 shows the parameters used to calculate the shear-wave reflection coefficient R_T for the oblique incidence of the shear wave with the spring interface model. We assume the same material properties for the axle and the wheel. The variation of R_T with the incident angle of the shear wave η_1 is shown in Fig. 9(a) for 2 MHz and Fig. 9(b) for 5 MHz.

Table 3. Parameters for spring interface model.

Frequency (MHz)	f	2	5
Angular frequency (rad/s)	ω	1.26×10^7	3.14×10^7
Shear wave incident angle (deg.)	η_1	0 to 90	
Longitudinal wave velocity (m/s)	c_L	5,915	
Shear wave velocity (m/s)	c_T	3,235	
Density (kg/m^3)	ρ	7,850	
Normal interfacial stiffness (N/m^3)	K_N	1.82×10^{15}	2.11×10^{15}
Tangential interfacial stiffness (N/m^3)	K_T	3.24×10^{14}	5.70×10^{14}
	K_T / K_N	0.178	0.270

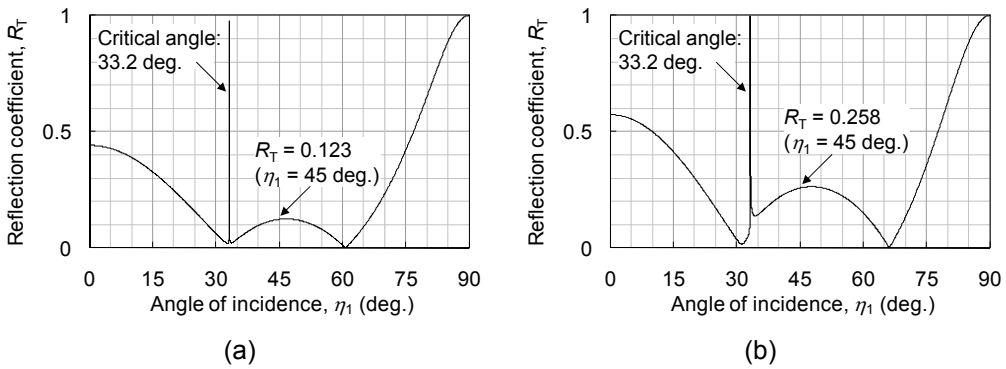

Fig. 9. The calculated reflection coefficient of the shear wave as a function of the angle of incidence, for (a) 2 MHz and (b) 5 MHz.

In Fig. 9, it is readily found that R_T is greater at 5 MHz than at 2 MHz within the range where the incident angle is smaller than around 60 degrees. This trend is found experimentally for the normal incidence as shown in Figs. 6 and 7. It is a natural outcome of the spring interface model when the interfacial stiffnesses are independent of the frequency, which still appears valid in the present case where the interfacial stiffnesses are assumed frequency-dependent.

The characteristics of the incident-angle dependence of the reflection coefficient can be summarized as follows: R_T shows a local minimum at η_1 of around 30 degrees, which coincides with the well-known fact that the incident shear wave changes its vibration mode from the shear wave to the longitudinal wave at around 30 degrees of the incident angle [20]. R_T approaches to 1 at η_1 of 33.3 degrees, which is slightly larger than the critical angle η_c of 33.2 degrees. R_T shows a local maximum at around 45 degrees. R_T is approximately equal to 0 at η_1 of 60.7 degrees at 2 MHz and of 66.2 degrees at 5 MHz. Then R_T again approaches to 1 with the angle η_1 approaching to 90 degrees.

The value of the reflection coefficient at the incident angle η_1 of 45 degrees, $R_{T,45deg}$, was 0.123 at 2 MHz and 0.258 at 5 MHz. On the decibel scale with $R_{T,dB} = 20 \log_{10}(R_{T,45deg})$, these values were –18.2 dB at 2 MHz and –11.8 dB at 5 MHz, respectively.

5. Discussions

5.1 Variation of reflection coefficient with interfacial stiffnesses

In Fig. 9, R_T shows a local maximum at around 45 degrees. For the shear wave incidence at 45 degrees, there is no reflected or transmitted longitudinal wave, as discussed by Margetan et al. [10], so the shear wave reflection is essentially determined by the normal stiffness K_N.

In Fig. 9, it is seen that R_T once becomes 0 at around 60 to 70 degrees, after R_T shows the local maximum and before it reaches 1 at $\eta_1 = 90$ degrees. Liaptsis et al. [18] reported a similar phenomenon for the oblique incidence of the longitudinal wave to the steel–steel interface. The situation that R_T becomes 0 is equivalent to $\bar{u}^{RT} = 0$ in Eq. (18) with n_1 replaced by in'_1. Then, rewriting Eq. (18) gives

$$\begin{bmatrix} -k_L\left(\lambda-2\mu n_1'^2\right) & 2k_T\mu\ell_1\ell_2 & k_L\left(\lambda-2\mu n_1'^2\right) & -2k_T\mu\ell_1\ell_2 \\ 2ik_L\mu n_1' n_2 & -k_T\mu\left(\ell_1^2-\ell_2^2\right) & 2ik_L\mu n_1' n_2 & k_T\mu\left(\ell_1^2-\ell_2^2\right) \\ iK_N n_1' & K_N\ell_2 & iK_N n_1' - ik_L\left(\lambda-2\mu n_1'^2\right) & -K_N\ell_2+2ik_T\mu\ell_1\ell_2 \\ -K_T n_2 & -K_T\ell_1 & K_T n_2+2k_L\mu n_1' n_2 & K_T\ell_1-ik_T\mu\left(\ell_1^2-\ell_2^2\right) \end{bmatrix} \begin{pmatrix} \bar{u}^{RL} \\ \bar{u}^{IT} \\ \bar{u}^{TL} \\ \bar{u}^{TT} \end{pmatrix} = \mathbf{0}. \tag{19}$$

The existence of an incident angle to give $\bar{u}^{RT} = 0$ is then governed by the condition that the determinant of the 4 × 4 matrix in Eq. (19) is zero, namely

$$\begin{aligned} &2\left[K_N k_T n_1'\left(\lambda-2\mu n_1'^2\right)\left(\ell_1^2-\ell_2^2\right)^2-8K_T k_T\mu n_1' n_2^2\ell_1^2\ell_2^2+2K_N k_L n_1' n_2\ell_2\left(\lambda-2\mu n_1'^2\right)\left(\ell_1^2-\ell_2^2\right)-4K_T k_L n_1' n_2\ell_1^2\ell_2\left(\lambda-2\mu n_1'^2\right)\right] \\ &-k_L k_T\left(\lambda-2\mu n_1'^2\right)^2\left(\ell_1^2-\ell_2^2\right)^2-16k_L k_T\mu^2 n_1'^2 n_2^2\ell_1^2\ell_2^2=0 \end{aligned} \tag{20}$$

Therefore, the angle of η_1 where $R_T = 0$ is determined by K_T, K_N and ω. In the following discussion, this angle is used to characterize the variation of the R_T–η_1 curve with the interfacial stiffnesses.

Here, we perform a parametric study to clarify the effect of K_N and K_T to the shape of the R_T–η_1 curve. We focus on the three characteristic points indicated in the center of Fig. 10; [A] local maximum of R_T, [B] the angle of η_1 where $R_T = 0$ and [C] the value of R_T at $\eta_1 = 0$ degrees. The results are summarized in Fig. 10. In this figure, the graph located at the center is the same as shown in Fig. 9(b) calculated for 5 MHz by using the interfacial stiffnesses K_N and K_T identified experimentally. In the following, we denote these reference values of the interfacial stiffnesses by $K_{N,exp}$ and $K_{T,exp}$, respectively, and the reference angular frequency by $\omega_{ref} = 3.14 \times 10^7$ rad/s, corresponding to the 5 MHz frequency. Based on the R_T–η_1 curve obtained by $K_{N,exp}$ and $K_{T,exp}$, the normal stiffness K_N is varied to $K_{N,exp}/2$, $K_{N,exp}$ and $2K_{N,exp}$ and the tangential stiffness K_T is varied to $K_{T,exp}/2$, $K_{T,exp}$ and $2K_{T,exp}$. For respective values of K_N and K_T, the R_T–η_1 curve is presented and the shift of the points of [A], [B] and [C] is shown in each graph by the indication with black arrows.

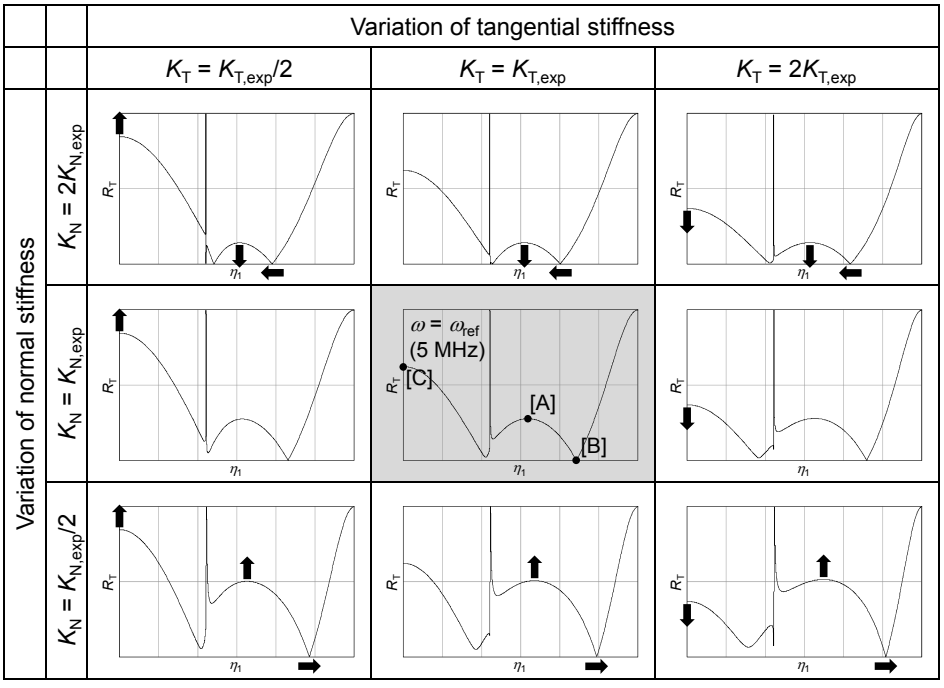

Fig. 10. The variation of the R_T–η_1 curve with the interfacial stiffnesses K_N and K_T.

The shift of the points of [A] and [B] clearly links to the variation of the normal stiffness K_N. When K_N becomes larger, e.g. $2K_{N,exp}$, the height [A] is lowered and the angle [B] is decreased. Also, the height [A] is nearly inversely proportional to K_N. The shift of the point [C] links to the variation of the tangential stiffness K_T. When K_T becomes larger, e.g. $2K_{T,exp}$, the height [C] is lowered and nearly inversely proportional to K_T.

There is a foregoing report that while the values of K_N and K_T become larger as the contact pressure at the interface becomes larger, K_T / K_N is kept approximately constant [18]. Now we consider the case where K_N varies with K_T / K_N and ω_{ref} kept constant, corresponding to the variation of the contact pressure. When K_N and K_T become larger simultaneously, i.e. $K_N = 2K_{N,exp}$ and $K_T = 2K_{T,exp}$, the heights of [A] and [C] are lowered and the angle [B] is decreased.

It is noted that the similar tendency is indicated by the parametric study if we select the reference angular frequency as $\omega_{ref} = 1.26 \times 10^7$ rad/s (2 MHz) with the corresponding interfacial stiffnesses $K_{N,exp}$ and $K_{T,exp}$ based on the R_T–η_l curve in Fig. 9(a).

5.2 Consideration for experimental results by applying spring interface model

Here, we discuss the ultrasonic test results of a miniature wheelset with a fatigue crack as mentioned in Section 2 by applying the spring interface model. Although it would be possible to model the contact behavior of the opposite faces of a fatigue crack by the normal and tangential springs with other specific stiffnesses, in this study we only focus on the contact effect of the axle–wheel interface. The contact behavior of the opposite crack faces is not discussed here since the present attention is given to the crack fully opened by the sufficient tensile stress caused by the bending moment.

Table 4 summarizes the experimental and calculated results of the relative decrease of the flaw echo height due to the fitted wheel. It is noted that, according to the recorded waveforms in the corner reflection of the axle end face, the peak frequency of the amplitude spectrum for the probes used in the experiment was 2.09 MHz by the 2 MHz probe and 4.51 MHz by the 5 MHz probe. In the following discussion, however, the nominal frequencies of the probes are dealt with as the representative ones governing the behavior of the ultrasound at the axle–wheel spring interface.

Table 4. Comparison of the relative decrease of the echo height between experimental and calculated results for each nominal frequency.

	Frequency of ultrasonic wave (MHz)			
	2		5	
	ratio	ratio in dB	ratio	ratio in dB
Experiment	0.221	–13.1	0.347	–9.2
Calculation (Spring interface model)	0.123	–18.2	0.258	–11.8

The experimental results in Table 4 show the relative decrease of the echo height due to the presence of the wheel for each nominal frequency of the probe used. We consider that the relative decrease of the

echo height corresponds to the reflection coefficient at the axle–wheel interface calculated by the spring interface model for the respective frequencies of 2 and 5 MHz. Since the relative decrease of the echo height was given by the ratio of echo heights with and without the wheel, the effect of the axle curvatures is considered to be cancelled out in this experiment, like in the measurement of the interfacial stiffnesses described above. Therefore, the curvature effect is not taken into account in the present discussion.

The calculated result shows that the flaw echo height at 5 MHz would decrease by approximately 11.8 dB when a wheel is fitted on the axle surface, while the echo-height decrease in the experiment was 9.2 dB. Similarly, the calculation for the echo-height decrease due to the presence of a wheel gives 18.2 dB at 2 MHz, where the experimental result was 13.1 dB. As a whole, it is considered that the present model gives a reasonable explanation for the relative decrease of the echo height due to the fitted wheel found in the experiment. In particular, the experimental finding showing greater relative decrease at lower frequency is qualitatively supported by the present theoretical analysis.

Some quantitative discrepancies found between the experimental and calculated results are discussed below, referring to the schematic view in Fig. 11. It is considered that the following two causes yielded the difference between the experimental and calculated results for each frequency.

(1) The effective interference of shrink fit is considered to be reduced due to the wear between the axle and the wheel during the fatigue loading. As a result, the contact pressure at the axle–wheel interface decreased and the effect of the presence of a wheel on the reflection coefficient was weakened, which is referred to in Figs. 11(a) and (b). In other words, the actual K_N and K_T values at the interface were decreased with the decrease of the contact pressure and the values of $K_{N,exp}$ and $K_{T,exp}$ were overestimated in the calculation.

(2) The stress distribution around the fatigue crack was varied by the nominal tensile stress of 165 MPa at the wheel seat by the applied bending moment. It caused the deformation of the axle around the edge of the wheel seat and decreased the contact pressure, or the effective interference, as shown in Fig. 11(c).

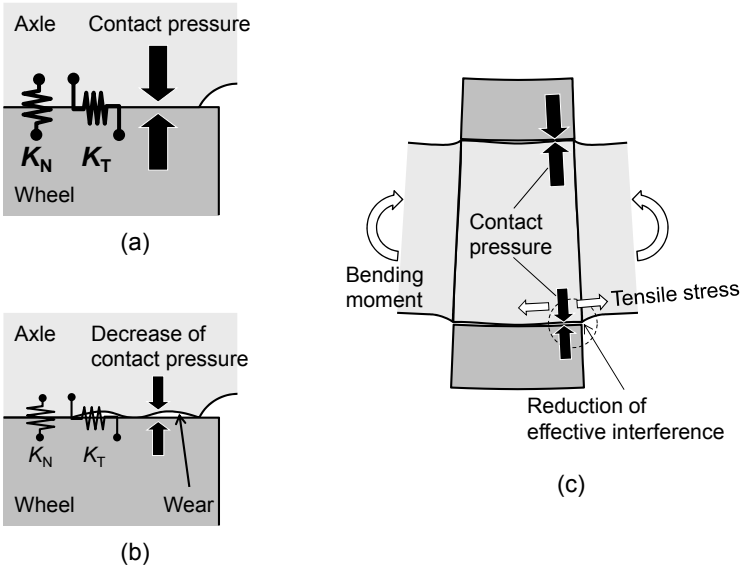

Fig. 11. Schematic illustrations of the axle–wheel interface (a) before and (b) after fatigue, and (c) the variation of stress distribution around the crack by the applied bending moment.

Contemplating the above inference, we attempt to adjust the values of K_N and K_T to fit the theoretical echo-height decrease at the incident angle of 45 degrees to the experimental results for each frequency of 2 and 5 MHz with the ratio K_T / K_N kept constant. Figure 12 shows the original and adjusted values of K_N and the fitted shape of the R_T–η_1 curve. To match the value of R_T with the echo-height decrease in the experiment, K_N should be 0.546 times of the original value of $K_{N,exp}$ for 2 MHz, and 0.723 times of the original value for 5 MHz. Provided that the interfacial stiffness is proportional to the contact pressure [7, 8], this fact suggests that the contact pressure between the axle and the wheel decreased by a factor of 0.5 to 0.7, in other words, decreased to the range of 46 to 61 MPa from the original value of approximately 85 MPa.

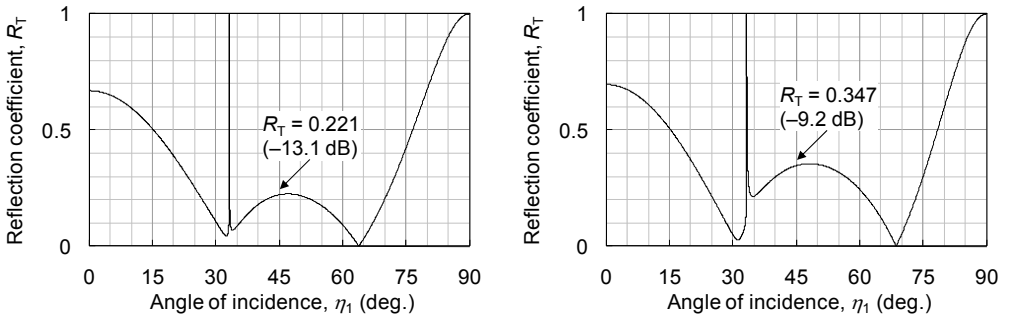

	R_T	K_N (N/m^3)	K_T (N/m^3)	K_T / K_N
Original	0.123	1.82×10^{15}	3.24×10^{14}	0.178
Adjusted	0.221	9.94×10^{14}	1.77×10^{14}	
K_N (Adjusted/Original)		0.546		

(a)

	R_T	K_N (N/m^3)	K_T (N/m^3)	K_T / K_N
Original	0.258	2.11×10^{15}	5.70×10^{14}	0.270
Adjusted	0.347	1.53×10^{15}	4.11×10^{14}	
K_N (Adjusted/Original)		0.723		

(b)

Fig. 12. Adjusted value of K_N with K_T / K_N kept constant to agree with the experimental result of the echo-height decrease at the incident angle of 45 degrees, for (a) 2 MHz and (b) 5 MHz.

6. Concluding remarks

The results obtained by this study can be summarized as follows.

The spring interface model was applied to the axle–wheel interface to explain the experimentally found decrease of the echo height of a fatigue crack due to the fitted wheel when probed by a shear-wave angle beam. The normal and tangential stiffnesses were identified experimentally from the normal-incidence reflection measurements, and then applied to analyze the shear-wave reflection behavior for the oblique incidence. The theoretical calculation qualitatively explained the decrease of the flaw echo height when the axle is fitted with a wheel.

Quantitatively, the theoretical results for the relative decrease of the echo height overestimate those obtained in the experiment. The causes of the difference between the experimental and calculated results were considered as (1) the reduction of the effective interference of shrink fit due to the wear during the fatigue loading, and (2) the variation of the stress distribution around the fatigue crack by the applied bending moment. For the estimated relative echo-height decrease to agree with the experimental results, K_N was found to be smaller than the value identified by the normal-incidence reflection measurement by a

factor of 0.5 to 0.7.

We used a miniature wheelset for this study instead of a full-sized wheelset. However, the obtained results provide some insights into the ultrasonic inspection of a full-sized axle or wheelset. One of the results mentioned above implies that, when using a 2 MHz probe for example, the flaw echo height will decrease by around 18 dB only by a fitted wheel on a crack. The amount of the echo-height decrease could be varied with the change of the fitting condition, which would be induced by the wear or the fretting. Although the influence might be slightly smaller when using a 5 MHz probe, the crack detectability would be undoubtedly deteriorated by the presence of a fitted wheel. It is noted that we should better be always aware of the influence of a fitted wheel on the inspection accuracy.

In this study, the contact behavior of the opposite faces of the fatigue crack is not taken into account. The theoretical modeling of the fatigue crack as well as the axle–wheel interface is one of our important future works. Further elaboration of such investigations as clarifying the factors quantitatively influencing the accuracy of the ultrasonic inspection should be carried out, which contributes to the progress of the further safety for the railway axles.

References

[1] H. Ishiduka, Probability of improvement in routine inspection work of Shinkansen vehicle axles, Q. Rep. Railw. Tech. Res. Inst. 40 (1999) 70–73.

[2] J. Yohso, Development of automatic ultrasonic testing equipment for general and bogie inspection of Shinkansen hollow axle, Proc. 11th Int. Wheelset Congr. vol. 2 (1995) 47–50.

[3] K. Makino, J. Yohso, H. Sakamoto, H. Ishiduka, Hollow axle ultrasonic crack detection for conventional railway vehicles, Q. Rep. Railw. Tech. Res. Inst. 46 (2005) 78–84.

[4] K. Makino, J. Yohso, H. Sakamoto, H. Ishiduka, An ultrasonic flaw detector for hollow axles of meter-gauge railway cars and results of axle fatigue test, Proc. 16th Int. Wheelset Congr. (2010) Session 7.4.

[5] K. Hirakawa, K. Toyama, M. Kubota, The analysis and prevention of failure in railway axles, Int. J. Fatig. 20 (1998) 135–144.

[6] T. Makino, T. Kato, K. Hirakawa, Review of the fatigue damage tolerance of high-speed railway axles in Japan, Eng. Fract. Mech. 78 (2011) 810–825.

[7] R. Lewis, M.B. Marshall, R.S. Dwyer-Joyce, Measurement of interface pressure in interference fits, Proc. Inst. Mech. Eng. Part C: J. Mech. Eng. Sci. 219 (2005) 127–139.

[8] M.B. Marshall, R. Lewis, R.S. Dwyer-Joyce, F. Demilly, Y. Flament, Ultrasonic measurement of railway wheel hub–axle press-fit contact pressures, Proc. Inst. Mech. Eng. Part F: J. Rail Rapid Transit 225 (2011) 287–298.

[9] K. Makino, S. Biwa, H. Sakamoto, J. Yohso, Ultrasonic evaluation of fatigue cracks at the wheel seat of a miniature wheelset, Nondestr. Test. Eval. 27 (2012) 29–46.

[10] F. J. Margetan, R.B. Thompson, T.A. Gray, Interfacial spring model for ultrasonic interactions with imperfect interfaces: Theory of oblique incidence and application to diffusion-bonded butt joints, J. Nondestr. Eval. 7 (1988) 131–152.

[11] A. Pilarski, J.L. Rose, A transverse-wave ultrasonic oblique-incidence technique for interfacial weakness detection in adhesive bonds, J. Appl. Phys. 63 (1988) 300–307.

[12] M. Schoenberg, Elastic wave behavior across linear slip interfaces, J. Acoust. Soc. Am. 68 (1980) 1516–1521.

[13] B.W. Drinkwater, R.S. Dwyer-Joyce, P. Cawley, A study of the interaction between ultrasound and a partially contacting solid–solid interface, Proc. R. Soc. Lond. A 452 (1996) 2613–2628.

[14] H.G. Tattersall, The ultrasonic pulse-echo technique as applied to adhesion testing, J. Phys. D: Appl. Phys. 6 (1973) 819–832.

[15] R.S. Dwyer-Joyce, B.W. Drinkwater, A.M. Quinn, The use of ultrasound in the investigation of rough surface interfaces, Trans. ASME 123 (2001) 8–16.

[16] S. Biwa, A. Suzuki, N. Ohno, Evaluation of interface wave velocity, reflection coefficients and interfacial stiffnesses of contacting surfaces, Ultrasonics 43 (2005) 495–502.

[17] J.R. Birchak, S. Serabian, Calibration of ultrasonic systems for inspection from curved surfaces, Mater. Eval. 36 (1978) 39–44.

[18] D. Liaptsis, B.W. Drinkwater, R. Thomas, The interaction of oblique incidence ultrasound with rough, partially contacting interfaces, Nondestr. Test. Eval. 21 (2006) 109–121.

[19] H.A. Sherif, S.S. Kossa, Relationship between normal and tangential contact stiffness of nominally flat surfaces, Wear 151 (1991) 49–62.

[20] C. Pecorari, A note on the sensitivity of SV wave scattering to surface-breaking cracks, Ultrasonics 43 (2005) 508–511.